Acta Mechanica Solida Sinica, Vol. 17, No. 3, September, 2004 ISSN 0894-9166
Published by AMSS Press, Wuhan, China. DOI: 10.1007/s10338-004-0433-8

AN ASSESSMENT OF THE MESHLESS WEIGHTED LEAST-SQUARE METHOD *

Pan Xiaofei[1] **Sze Kim Yim**[2] **Zhang Xiong**[1]
([1] *Department of Engineering Mechanics, Tsinghua Univesity, Beijing* 100084, *China*)
([2] *Department of Mechanical Engineering, The University of Hong Kong, Pokfulam Road, Hong Kong SAR, China*)

Received 18 July 2003; revision received 20 April 2004.

ABSTRACT The meshless weighted least-square (MWLS) method was developed based on the weighted least-square method. The method possesses several advantages, such as high accuracy, high stability and high efficiency. Moreover, the coefficient matrix obtained is symmetric and semi-positive definite. In this paper, the method is further examined critically. The effects of several parameters on the results of MWLS are investigated systematically by using a cantilever beam and an infinite plate with a central circular hole. The numerical results are compared with those obtained by using the collocation-based meshless method (CBMM) and Galerkin-based meshless method (GBMM). The investigated parameters include the type of approximations, the type of weight functions, the number of neighbors of an evaluation point, as well as the manner in which the neighbors of an evaluation point are determined. This study shows that the displacement accuracy and convergence rate obtained by MWLS is comparable to that of the GBMM while the stress accuracy and convergence rate yielded by MWLS is even higher than that of GBMM. Furthermore, MWLS is much more efficient than GBMM.

This study also shows that the instability of CBMM is mainly due to the neglect of the equilibrium residuals at boundary nodes. In MWLS, the residuals of all the governing equations are minimized in a weighted least-square sense.

KEY WORDS meshless, meshfree, least-square, weighted residual

I. INTRODUCTION

The finite element method (FEM) has been the most frequently used and powerful numerical method for engineering analysis for the last thirty years. However, mesh generation required in FEM can be a very time-consuming and expensive task. Furthermore, mesh-based methods are not well suited to the problems associated with severe deformation which requires frequent remeshing. In recent years, considerable effort has been devoted to the development of the so-called meshless methods and more than 10 different versions have been proposed[1--3]. Meshless methods have been successful in solving high velocity impact[4,5], dynamic fracture[6], metal forming[7], localization[8] and jointed rock structures[9], just to mention a few.

Two discretization methods, the collocation method and Galerkin method, have been dominant in the existing meshless methods. In fact, all meshless methods could be obtained from the weighted residual method. In the Galerkin method, derivatives in domain integrals are lowered by using the divergence theorem to establish the weak form. The inaccuracy in integrating the weak form will result

* Project supported by the National Natural Science Foundation of China (No.10172052).

in significant error in the solution. However, the shape functions in meshless method are very complex. Delicate background integration cells and a large number of quadrature points must generally be employed to evaluate the weak form as accurately as possible[10]. As a consequence, the Galerkin-based meshless methods are much more expensive than FEM. In contrast, collocation-based meshless methods are truly meshless and very efficient. Equilibrium conditions are satisfied only at the nodes within the problem domain neither than at the boundary nodes. Hence, significant error can result. These methods also suffer from instability. Recently, Zhang et al. have proposed a Least-Square Collocation Meshless (LSCM) method[11]. In addition to the nodes used to construct the trial functions, a number of auxiliary points are also used in LSCM. Unlike the conventional collocation method, the equilibrium equations are taken not only at the nodes within the domain but also at the boundary nodes. Together with the equations arising from the boundary conditions, the total number of equations exceeds the number of unknowns and the system of equations was solved in the least-square sense. Numerical studies showed that LSCM are stable, efficient and highly accurate. Similar to the conventional collocation method, the coefficient matrix detailing the system of equations is unsymmetric.

The Least-square method is a well-known weighted residual method[12]. In the least-squares method, integration is only used to average the residual of the governing equations. The solution accuracy in the least-square method is less sensitive to the integration accuracy than in the Galerkin method. Consequently, it is possible to use a very simple integration scheme in a least-square-based meshless method to improve the efficiency of the related meshless method. Based on the least-square method, a very efficient truly meshless method, meshless weighted least-square method, was proposed in Ref.[13]. MWLS possesses several advantages. The residual of the governing equations is averaged in MWLS so that it is much more accurate and stable than collocation-based methods. No integration is involved in MWLS so that it is much more efficient than Galerkin-based meshless methods. The coefficient matrix of the resulting equations is semi-definite and symmetric. Like all collocation methods, MWLS requires the calculation of second order derivatives that would typically not be required in a Galerkin-based meshless method.

MWLS is critically examined in this paper. Many parameters have pronounced effects on the results of meshless methods such as the type of approximation, the type of the weight function and the manner in which the neighbors of an evaluation point are determined. The effects of these parameters on the MWLS, CBMM and GBMM are investigated carefully. Numerical studies show that the displacement accuracy obtained by MWLS is comparable to that of GBMM yet the stress accuracy yielded by MWLS is even higher than that of GBMM. In MWLS, the accuracy of displacement and stress appears to be in the same order of magnitude. However, the accuracy of displacement seems to be one order lower than that of stress in GBMM. Evidently, MWLS is much more efficient than GBMM and is a promising truly meshless method.

A brief description of the moving least-square (MLS) approximation and standard least-square (LSQ) approximation is presented in §II. In §III, the formulation of MWLS is briefly reviewed, and attention is paid to the difference between the meshless weighted least-square method and collocation-based meshless method. MWLS, CBMM and GBMM are examined critically in §IV by using two numerical examples which are a cantilever beam and the infinite plate with a central circular hole. The paper ends with the concluding remarks made in §V.

II. MOVING LEAST-SQUARE APPROXIMATION AND LEAST-SQUARE APPROXIMATION

In MLS approximation, the function $u(\boldsymbol{x})$ is approximated in domain Ω by $\widehat{u}(\boldsymbol{x})$, namely,

$$u(\boldsymbol{x}) \approx \widehat{u}(\boldsymbol{x}) = \sum_{i=1}^{m} p_i(\boldsymbol{x}) \cdot a_i(\boldsymbol{x}) = \boldsymbol{p}^{\mathrm{T}}(\boldsymbol{x}) \cdot \boldsymbol{a}(\boldsymbol{x}) \tag{1}$$

where $p_i(\boldsymbol{x})$ are monomial basis functions, $a_i(\boldsymbol{x})$ are their coefficients and m is the number of terms in the basis. The coefficients $a_i(\boldsymbol{x})$ are obtained by minimizing the functional $J(\boldsymbol{x})$ given by

$$J(\boldsymbol{x}) = \sum_{I=1}^{k} w_I(\boldsymbol{x}) \cdot \left[\sum_{i=1}^{m} p_i(\boldsymbol{x}_I) \cdot a_i(\boldsymbol{x}) - u_I \right]^2 \tag{2}$$

where $u_I = u(\boldsymbol{x}_I)$ is the nodal value of $u(\boldsymbol{x})$ at node $\boldsymbol{x}_I$, $w_I(\boldsymbol{x}) = w(\boldsymbol{x} - \boldsymbol{x}_I)$ is a non-negative weight function with compact support associated with node $\boldsymbol{x}_I$ and maximum at node $\boldsymbol{x}_I$. Moreover, k is the total number of nodes at which the weight function $w_I(\boldsymbol{x})$ does not vanish. Minimizing Eq.(2) for $a_i(\boldsymbol{x})$, and then substituting $a_i(\boldsymbol{x})$ into Eq.(1) lead to

$$u(\boldsymbol{x}) \approx \widehat{u}(\boldsymbol{x}) = \boldsymbol{\phi}^{\mathrm{T}}(\boldsymbol{x}) \cdot \boldsymbol{u} \tag{3}$$

where the shape function matrix $\boldsymbol{\phi}(\boldsymbol{x})$ is given by

$$\boldsymbol{\phi}^{\mathrm{T}}(\boldsymbol{x}) = \boldsymbol{p}^{\mathrm{T}}(\boldsymbol{x}) \cdot \boldsymbol{A}^{-1}(\boldsymbol{x}) \cdot \boldsymbol{B}(\boldsymbol{x}) \tag{4}$$

and

$$\boldsymbol{A}(\boldsymbol{x}) = \sum_{I=1}^{k} w_I(\boldsymbol{x}) \boldsymbol{p}(\boldsymbol{x}_I) \boldsymbol{p}^{\mathrm{T}}(\boldsymbol{x}_I) \tag{5}$$

$$\boldsymbol{B}(\boldsymbol{x}) = [w_1(\boldsymbol{x})\boldsymbol{p}(\boldsymbol{x}_1),\ w_2(\boldsymbol{x})\boldsymbol{p}(\boldsymbol{x}_2),\ \cdots,\ w_k(\boldsymbol{x})\boldsymbol{p}(\boldsymbol{x}_k)] \tag{6}$$

$$\boldsymbol{u} = \{u_1,\ u_2,\ \cdots,\ u_k\}^{\mathrm{T}} \tag{7}$$

The first and second order of derivatives of the shape function can be obtained as

$$\begin{aligned} \boldsymbol{\phi}_{,i}^{\mathrm{T}} &= \boldsymbol{r}_{,i}^{\mathrm{T}} \cdot \boldsymbol{B} + \boldsymbol{r}^{\mathrm{T}} \cdot \boldsymbol{B}_{,i} \\ \boldsymbol{\phi}_{,ij}^{\mathrm{T}} &= \boldsymbol{r}_{,ij}^{\mathrm{T}} \cdot \boldsymbol{B} + \boldsymbol{r}_{,i}^{\mathrm{T}} \cdot \boldsymbol{B}_{,j} + \boldsymbol{r}_{,j}^{\mathrm{T}} \cdot \boldsymbol{B}_{,i} + \boldsymbol{r}^{\mathrm{T}} \cdot \boldsymbol{B}_{,ij} \end{aligned} \tag{8}$$

where $\boldsymbol{r}^{\mathrm{T}}(\boldsymbol{x}) = \boldsymbol{p}^{\mathrm{T}}(\boldsymbol{x}) \cdot \boldsymbol{A}^{-1}(\boldsymbol{x})$, subscript i denotes the derivative with respect to coordinate x_i. The derivatives of $\boldsymbol{r}$ are given by

$$\begin{aligned} \boldsymbol{r}_{,i} &= \boldsymbol{A}^{-1}(\boldsymbol{p}_{,i} - \boldsymbol{A}_{,i}\boldsymbol{r}) \\ \boldsymbol{r}_{,ij} &= \boldsymbol{A}^{-1}(\boldsymbol{p}_{,ij} - \boldsymbol{A}_{,i}\boldsymbol{r}_{,j} - \boldsymbol{A}_{,j}\boldsymbol{r}_{,i} - \boldsymbol{A}_{,ij}\boldsymbol{r}) \end{aligned} \tag{9}$$

If the weight function, $w_I(\boldsymbol{x})$, together with its first l derivatives are continuous, the MLS shape functions in $\boldsymbol{\phi}(\boldsymbol{x})$ and their first l derivatives are also continuous. Hence, the weight function plays an important role in the performance of the MLS approximation. The effects of the following 8 weight functions on the results of meshless methods will be investigated. In all functions, $r = \|\boldsymbol{x}_I - \boldsymbol{x}\| / d_{mI}$ and d_{mI} is the support radius of node I.

1. WF1 (Gaussian)

$$w(r) = \begin{cases} \dfrac{\mathrm{e}^{-\beta^2 r^2} - \mathrm{e}^{-\beta^2}}{1 - \mathrm{e}^{-\beta^2}} & (r \le 1) \\ 0 & (\text{otherwise}) \end{cases} \tag{10}$$

where β is a constant.

2. WF2 (exponential)

$$w(r) = \begin{cases} \mathrm{e}^{-(r/\alpha)^2} & (0 \le r \le 1) \\ 0 & (\text{otherwise}) \end{cases} \tag{11}$$

where α is a constant.

3. WF3

$$w(r) = \begin{cases} 1 - 6r^2 + 8r^3 - 3r^4 & (0 \le r \le 1) \\ 0 & (\text{otherwise}) \end{cases} \tag{12}$$

4. WF4

$$w(r) = \begin{cases} 1 - 10r^3 + 15r^4 - 6r^5 & (0 \le r \le 1) \\ 0 & (\text{otherwise}) \end{cases} \tag{13}$$

5. WF5

$$w(r) = \begin{cases} \dfrac{2}{3} - 4r^2 + 4r^3 & (0 \le r < 0.5) \\ \dfrac{4}{3} - 4r + 4r^2 - \dfrac{4}{3}r^3 & (0.5 \le r \le 1) \\ 0 & (\text{otherwise}) \end{cases} \tag{14}$$

6. WF6

$$w(r) = \begin{cases} 1 - 3r^2 + 2r^3 & (0 \le r \le 1) \\ 0 & (\text{otherwise}) \end{cases} \tag{15}$$

7. WF7

$$w(r) = \begin{cases} 1 - 2r^2 & (0 \le r < 0.5) \\ 2(1-r)^2 & (0.5 \le r \le 1) \\ 0 & (\text{otherwise}) \end{cases} \tag{16}$$

8. WF8

$$w(r) = \begin{cases} (1 - r^2)^n & (0 \le r \le 1) \\ 0 & (\text{otherwise}) \end{cases} \tag{17}$$

where $n \ge 2$ and is set to 2 in this paper.

It is trivial to show that all the functions are at least first oder continuous. In this paper, the support radius d_{mI} of node I is determined by $\chi \cdot s[k]$, where $s[k]$ is the distance between node I and its k-th closest nodes and χ a scale. There are usually more than k nodes whose supports cover point $\boldsymbol{x}$, i.e. $w_I(\boldsymbol{x}) > 0$, but only the first k nodes closest to point $\boldsymbol{x}$ are used to construct the MLS approximation at point $\boldsymbol{x}$. In other words, the domain $\Omega_{\boldsymbol{x}}$ of definition of point $\boldsymbol{x}$ is the union of the k overlapping circles, each centered at $\boldsymbol{x}_I (I = 1, 2, \cdots, k)$ and of radius d_{mI}. Parameter χ controls the span of weight function[13].

The approximation of function $u(\boldsymbol{x})$ can also be established by using the least-square (LSQ) approximation. The LSQ approximation is constructed by minimizing the functional $J(\boldsymbol{x})$ given by

$$J(\boldsymbol{x}) = \sum_{I=1}^{k} \left[\sum_{i=1}^{m} p_i(\boldsymbol{x}_I) \cdot a_i(\boldsymbol{x}) - u_I \right]^2 \tag{18}$$

Minimizing Eq.(18) for $a_i(\boldsymbol{x})$, and then, substituting $a_i(\boldsymbol{x})$ into Eq.(1), we obtain the LSQ shape function matrix in the same form as (4) with

$$\boldsymbol{A} = \sum_{I=1}^{k} \boldsymbol{p}(\boldsymbol{x}_I) \boldsymbol{p}^{\mathrm{T}}(\boldsymbol{x}_I) \tag{19}$$

$$\boldsymbol{B} = [\boldsymbol{p}(\boldsymbol{x}_1),\ \boldsymbol{p}(\boldsymbol{x}_2),\ \cdots,\ \boldsymbol{p}(\boldsymbol{x}_k)] \tag{20}$$

The first and second order of derivatives of the shape function can be obtained as

$$\boldsymbol{\phi}_{,i}^{\mathrm{T}} = \boldsymbol{r}_{,i}^{\mathrm{T}} \cdot \boldsymbol{B}, \qquad \boldsymbol{\phi}_{,ij}^{\mathrm{T}} = \boldsymbol{r}_{,ij}^{\mathrm{T}} \cdot \boldsymbol{B} \tag{21}$$

where the derivatives of $\boldsymbol{r}$ are given by

$$\boldsymbol{r}_{,i} = \boldsymbol{A}^{-1} \boldsymbol{p}_{,i}, \qquad \boldsymbol{r}_{,ij} = \boldsymbol{A}^{-1} \boldsymbol{p}_{,ij} \tag{22}$$

It should be noted that the computational effort required for evaluating the LSQ shape functions and their derivatives is much less than that of the MLS shape functions and their derivatives. However, meshless methods using LSQ approximation is very sensitive to the neighbors of the evaluation point[14]. In applications such as high velocity impact and explosion, a large number of nodes are usually required to model the wave propagation properly and, thus, LSQ is a sensible approximation to reduce the computational cost.

III. MESHLESS WEIGHTED LEAST-SQUARES AND COLLOCATION BASED MESHLESS METHOD

Consider the 2D static elasticity problem

$$\begin{aligned} &\boldsymbol{L}[\boldsymbol{u}(\boldsymbol{x})] + \boldsymbol{f}(\boldsymbol{x}) = 0 && (\boldsymbol{x} \in \Omega) \\ &\boldsymbol{u}(\boldsymbol{x}) = \bar{\boldsymbol{u}}(\boldsymbol{x}) && (\boldsymbol{x} \in \Gamma_u) \\ &\boldsymbol{T}[\boldsymbol{u}(\boldsymbol{x})] = \bar{\boldsymbol{t}}(\boldsymbol{x}) && (\boldsymbol{x} \in \Gamma_t) \end{aligned} \tag{23}$$

where $\boldsymbol{u}(\boldsymbol{x})$ is the displacement field to be solved. $\boldsymbol{f}(\boldsymbol{x})$, $\bar{\boldsymbol{u}}(\boldsymbol{x})$, and $\bar{\boldsymbol{t}}(\boldsymbol{x})$ are prescribed functions defined in domain Ω, boundary Γ_u and boundary Γ_t, respectively. The differential operators $\boldsymbol{L}$ and $\boldsymbol{T}$ are given by

$$\boldsymbol{L} = \frac{E}{1-\nu^2}\begin{bmatrix} \dfrac{\partial^2}{\partial x^2} + \dfrac{1-\nu}{2}\dfrac{\partial^2}{\partial y^2} & \dfrac{1+\nu}{2}\dfrac{\partial^2}{\partial x \partial y} \\ \dfrac{1+\nu}{2}\dfrac{\partial^2}{\partial x \partial y} & \dfrac{\partial^2}{\partial y^2} + \dfrac{1-\nu}{2}\dfrac{\partial^2}{\partial x^2} \end{bmatrix} \tag{24}$$

$$\boldsymbol{T} = \frac{E}{1-\nu^2}\begin{bmatrix} l\dfrac{\partial}{\partial x} + m\dfrac{1-\nu}{2}\dfrac{\partial}{\partial y} & l\nu\dfrac{\partial}{\partial y} + m\dfrac{1-\nu}{2}\dfrac{\partial}{\partial x} \\ m\nu\dfrac{\partial}{\partial x} + l\dfrac{1-\nu}{2}\dfrac{\partial}{\partial y} & m\dfrac{\partial}{\partial y} + l\dfrac{1-\nu}{2}\dfrac{\partial}{\partial x} \end{bmatrix} \tag{25}$$

where l and m are the direction cosines of the outward normal to the boundary Γ_t. E and ν are the Young's modulus and Poisson's ratio, respectively.

MWLS was developed[13] based on the least-square variational principles[15]. The functional was established in a simplified discrete form for the 2D static elasticity problem as[13]

$$\begin{aligned} \Pi = & \sum_{i=1}^{N} \{\boldsymbol{L}[\hat{\boldsymbol{u}}(\boldsymbol{x}_i)] + \boldsymbol{f}(\boldsymbol{x}_i)\}^{\mathrm{T}} \cdot \{\boldsymbol{L}[\hat{\boldsymbol{u}}(\boldsymbol{x}_i)] + \boldsymbol{f}(\boldsymbol{x}_i)\} \\ & + \sum_{j=1}^{N_u} \lambda_u [\hat{\boldsymbol{u}}(\boldsymbol{x}_j) - \bar{\boldsymbol{u}}(\boldsymbol{x}_j)]^{\mathrm{T}} \cdot [\hat{\boldsymbol{u}}(\boldsymbol{x}_j) - \bar{\boldsymbol{u}}(\boldsymbol{x}_j)] \\ & + \sum_{k=1}^{N_t} \lambda_t \{\boldsymbol{T}[\hat{\boldsymbol{u}}(\boldsymbol{x}_k)] - \bar{\boldsymbol{t}}(\boldsymbol{x}_k)\}^{\mathrm{T}} \cdot \{\boldsymbol{T}[\hat{\boldsymbol{u}}(\boldsymbol{x}_k)] - \bar{\boldsymbol{t}}(\boldsymbol{x}_k)\} \end{aligned} \tag{26}$$

where $\hat{\boldsymbol{u}}(\boldsymbol{x}_i)$ is the trial function, N the total number of nodes, N_u the total number of nodes located on boundary Γ_u and N_t the total number of nodes located on boundary Γ_t. Moreover, λ_u and λ_t are penalty functions for imposing the boundary conditions. In this paper, $\lambda_t = 10^5$ and $\lambda_u = \lambda_t[E/(1-\nu^2)]^2$.

Substituting the MLS approximation (3) into Eq.(26) and then minimizing the functional Π with respect to $\boldsymbol{u}$ result in

$$\boldsymbol{K}\boldsymbol{U} = \boldsymbol{P} \tag{27}$$

where

$$\boldsymbol{K} = \sum_{i=1}^{N} \boldsymbol{H}_i^{\mathrm{T}} \boldsymbol{H}_i + \sum_{j=1}^{N_u} \lambda_u \boldsymbol{N}_j^{\mathrm{T}} \boldsymbol{N}_j + \sum_{k=1}^{N_t} \lambda_t \boldsymbol{Q}_k^{\mathrm{T}} \boldsymbol{Q}_k \tag{28}$$

$$\boldsymbol{P} = -\sum_{i=1}^{N} \boldsymbol{H}_i^{\mathrm{T}} \boldsymbol{f} + \sum_{j=1}^{N_u} \lambda_u \boldsymbol{N}_j^{\mathrm{T}} \bar{\boldsymbol{u}} + \sum_{k=1}^{N_t} \lambda_t \boldsymbol{Q}_k^{\mathrm{T}} \bar{\boldsymbol{t}} \tag{29}$$

$$\boldsymbol{U} = \{u_1,\ u_2,\ \cdots,\ u_N\}^{\mathrm{T}} \tag{30}$$

In Eqs.(28) and (29),

$$\boldsymbol{N}_i = \begin{bmatrix} \varphi_1 & 0 & \varphi_2 & 0 & \cdots & \varphi_N & 0 \\ 0 & \varphi_1 & 0 & \varphi_2 & \cdots & 0 & \varphi_N \end{bmatrix}_{(x_i, y_i)} \tag{31}$$

$$\begin{aligned} \boldsymbol{H}_i &= \boldsymbol{L}(\boldsymbol{N}_i) \\ &= E' \begin{bmatrix} \dfrac{\partial^2 \varphi_1}{\partial x^2} + \dfrac{1-\nu}{2}\dfrac{\partial^2 \varphi_1}{\partial y^2} & \dfrac{1+\nu}{2}\dfrac{\partial^2 \varphi_1}{\partial x \partial y} & \cdots \\ \dfrac{1+\nu}{2}\dfrac{\partial^2 \varphi_1}{\partial x \partial y} & \dfrac{\partial^2 \varphi_1}{\partial y^2} + \dfrac{1-\nu}{2}\dfrac{\partial^2 \varphi_1}{\partial x^2} & \cdots \\ \dfrac{\partial^2 \varphi_N}{\partial x^2} + \dfrac{1-\nu}{2}\dfrac{\partial^2 \varphi_N}{\partial y^2} & \dfrac{1+\nu}{2}\dfrac{\partial^2 \varphi_N}{\partial x \partial y} & \\ \dfrac{1+\nu}{2}\dfrac{\partial^2 \varphi_N}{\partial x \partial y} & \dfrac{\partial^2 \varphi_N}{\partial y^2} + \dfrac{1-\nu}{2}\dfrac{\partial^2 \varphi_N}{\partial x^2} & \end{bmatrix}_{(x_i, y_i)} \end{aligned} \tag{32}$$

$$\begin{aligned}\boldsymbol{Q}_i &= \boldsymbol{T}(\boldsymbol{N}_i) \\ &= E' \begin{bmatrix} l\dfrac{\partial\varphi_1}{\partial x} + m\dfrac{1-\nu}{2}\dfrac{\partial\varphi_1}{\partial y} & l\nu\dfrac{\partial\varphi_1}{\partial y} + m\dfrac{1-\nu}{2}\dfrac{\partial\varphi_1}{\partial x} & \cdots \\ m\nu\dfrac{\partial\varphi_1}{\partial x} + l\dfrac{1-\nu}{2}\dfrac{\partial\varphi_1}{\partial y} & m\dfrac{\partial\varphi_1}{\partial y} + l\dfrac{1-\nu}{2}\dfrac{\partial\varphi_1}{\partial x} & \cdots \\ l\dfrac{\partial\varphi_N}{\partial x} + m\dfrac{1-\nu}{2}\dfrac{\partial\varphi_N}{\partial y} & l\nu\dfrac{\partial\varphi_N}{\partial y} + m\dfrac{1-\nu}{2}\dfrac{\partial\varphi_N}{\partial x} & \\ m\nu\dfrac{\partial\varphi_N}{\partial x} + l\dfrac{1-\nu}{2}\dfrac{\partial\varphi_N}{\partial y} & m\dfrac{\partial\varphi_N}{\partial y} + l\dfrac{1-\nu}{2}\dfrac{\partial\varphi_N}{\partial x} & \end{bmatrix}_{(x_i,y_i)}\end{aligned} \tag{33}$$

where $E' = E/(1-\nu^2)$.

In CBMM, the equilibrium equation is satisfied at every node within the domain Ω, the prescribed displacement condition is satisfied at every node located on boundary Γ_u and the prescribed traction boundary condition is satisfied at every node located on boundary Γ_t, namely

$$\begin{aligned} &\boldsymbol{L}[\hat{\boldsymbol{u}}(\boldsymbol{x}_i)] + \boldsymbol{f}(\boldsymbol{x}_i) = 0 \quad (\boldsymbol{x}_i \in \Omega) \quad (i = 1, 2, \cdots, N - N_u - N_t) \\ &\hat{\boldsymbol{u}}(\boldsymbol{x}_i) = \bar{\boldsymbol{u}}(\boldsymbol{x}_i) \quad (\boldsymbol{x}_i \in \Gamma_u) \quad (i = 1, 2, \cdots, N_u) \\ &\boldsymbol{T}[\hat{\boldsymbol{u}}(\boldsymbol{x}_i)] = \bar{\boldsymbol{t}}(\boldsymbol{x}_i) \quad (\boldsymbol{x}_i \in \Gamma_t) \quad (i = 1, 2, \cdots, N_t)\end{aligned} \tag{34}$$

Substituting Eq.(3) into Eqs.(34) leads to

$$\begin{bmatrix} \boldsymbol{H} \\ \boldsymbol{N} \\ \boldsymbol{Q} \end{bmatrix} \boldsymbol{U} = \begin{Bmatrix} \boldsymbol{f} \\ \bar{\boldsymbol{u}} \\ \bar{\boldsymbol{t}} \end{Bmatrix} \tag{35}$$

where $\boldsymbol{H} = [\boldsymbol{H}_1^{\mathrm{T}},\ \boldsymbol{H}_2^{\mathrm{T}},\ \cdots, \boldsymbol{H}_{N-N_u-N_t}^{\mathrm{T}}]^{\mathrm{T}}$, $\boldsymbol{N} = [\boldsymbol{N}_1^{\mathrm{T}},\ \boldsymbol{N}_2^{\mathrm{T}},\ \cdots,\ \boldsymbol{N}_{N_u}^{\mathrm{T}}]^{\mathrm{T}}$, $\boldsymbol{Q} = [\boldsymbol{Q}_1^{\mathrm{T}},\ \boldsymbol{Q}_2^{\mathrm{T}},\ \cdots, \boldsymbol{Q}_{N_t}^{\mathrm{T}}]^{\mathrm{T}}$. There are N equations with N unknowns in Eq.(35), and the coefficient matrix is nonsymmetric. Multiplying the second equation of Eq.(35) by $\sqrt{\lambda_u}$, the third equation of Eq.(35) by $\sqrt{\lambda_t}$, and then premultiplying Eq.(35) by $[\boldsymbol{H}^{\mathrm{T}},\ \sqrt{\lambda_u}\boldsymbol{N}^{\mathrm{T}},\ \sqrt{\lambda_t}\boldsymbol{Q}^{\mathrm{T}}]$, results in a equation in the same form as Eq.(27) with matrices $\boldsymbol{K}$ and $\boldsymbol{P}$ given by

$$\boldsymbol{K} = \sum_{i=1}^{N-N_u-N_t} \boldsymbol{H}_i^{\mathrm{T}}\boldsymbol{H}_i + \sum_{j=1}^{N_u} \lambda_u \boldsymbol{N}_j^{\mathrm{T}}\boldsymbol{N}_j + \sum_{k=1}^{N_t} \lambda_t \boldsymbol{Q}_k^{\mathrm{T}}\boldsymbol{Q}_k \tag{36}$$

$$\boldsymbol{P} = -\sum_{i=1}^{N-N_u-N_t} \boldsymbol{H}_i^{\mathrm{T}}\boldsymbol{f} + \sum_{j=1}^{N_u} \lambda_u \boldsymbol{N}_j^{\mathrm{T}}\bar{\boldsymbol{u}} + \sum_{k=1}^{N_t} \lambda_t \boldsymbol{Q}_k^{\mathrm{T}}\bar{\boldsymbol{t}} \tag{37}$$

If the residuals of equilibrium equations of boundary nodes are excluded from the functional Π given in Eq.(26), the matrices $\boldsymbol{K}$ and $\boldsymbol{P}$ given in Eqs.(28) and (29) are the same as those given in Eqs.(36) and (37). That is to say, the essential difference between MWLS and CBMM is how to deal with the residual of equilibrium equations at boundary nodes. In CBMM, equilibrium conditions are satisfied exactly at the nodes within the domain Ω but are ignored at the nodes on boundary Γ_u and boundary Γ_t. In MWLS, the summation of weighted squared residuals of all governing equations at all nodes is minimized. In other words, the equilibrium conditions are satisfied at all nodes in a weighted least squares sense. If the residuals of equilibrium equations at the boundary nodes are ignored in Eq.(26), MWLS should yield the same results as those given by CBMM.

IV. ASSESSMENT OF THE MESHLESS WEIGHTED LEAST-SQUARE METHOD

When MLS is used to construct the meshless approximation function, the weight function plays a important role. In this section, two numerical examples, a cantilever beam and an infinite plate with a central circular hole, are used to investigate the effects of the following parameters on the results of MWLS, CBMM and GBMM:

1. Type of meshless approximation: MLS and LSQ;

2. Number of nodes, k, used to construct the meshless approximation;
3. Type of weighted functions used in MLS;
4. Parameter β in the weight function WF1 and parameter α in WF2.
5. Parameter χ, which controls the span of the weight function;

Quadratic basis is used in all analyses. For the purpose of error estimation and convergence studies, the following error norms are calculated

$$L_u = \frac{\sqrt{\sum_{i=1}^{N}(\hat{\boldsymbol{u}}_i - \boldsymbol{u}_i)^{\mathrm{T}} \cdot (\hat{\boldsymbol{u}}_i - \boldsymbol{u}_i)}}{\sqrt{\sum_{i=1}^{N} \boldsymbol{u}_i^{\mathrm{T}} \cdot \boldsymbol{u}_i}} \times 100\%, \qquad L_\sigma = \frac{\sqrt{\sum_{i=1}^{N}(\hat{\boldsymbol{\sigma}}_i - \boldsymbol{\sigma}_i)^{\mathrm{T}} \cdot (\hat{\boldsymbol{\sigma}}_i - \boldsymbol{\sigma}_i)}}{\sqrt{\sum_{i=1}^{N} \boldsymbol{\sigma}_i^{\mathrm{T}} \cdot \boldsymbol{\sigma}_i}} \times 100\% \quad (38)$$

where N is the total number of nodes, $\hat{\boldsymbol{u}}_i$ and $\boldsymbol{u}_i$ are the approximation and exact displacement values at point $\boldsymbol{x}_i$, $\hat{\boldsymbol{\sigma}}_i$ and $\boldsymbol{\sigma}_i$ are the approximation and exact stress value at point $\boldsymbol{x}_i$.

4.1. Cantilever Beam

Consider a cantilever beam subject to end load P as shown in Fig. 1(a). The exact solution of this problem is given by Timoshenko and Goodier[16,11]. In this analysis, dimensionless Young's modulus $E = 10000$, Poisson's ratio $\nu = 1/3$, $P = 6$, $D = 2$, $L = 12$. 9×33 regular nodes, as shown in Fig. 1(b), are used.

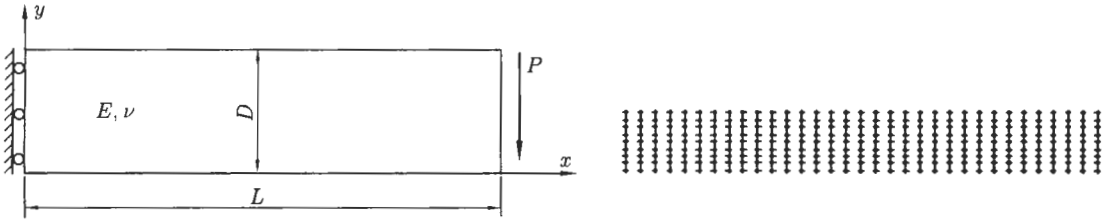

Fig. 1. Cantilever beam.

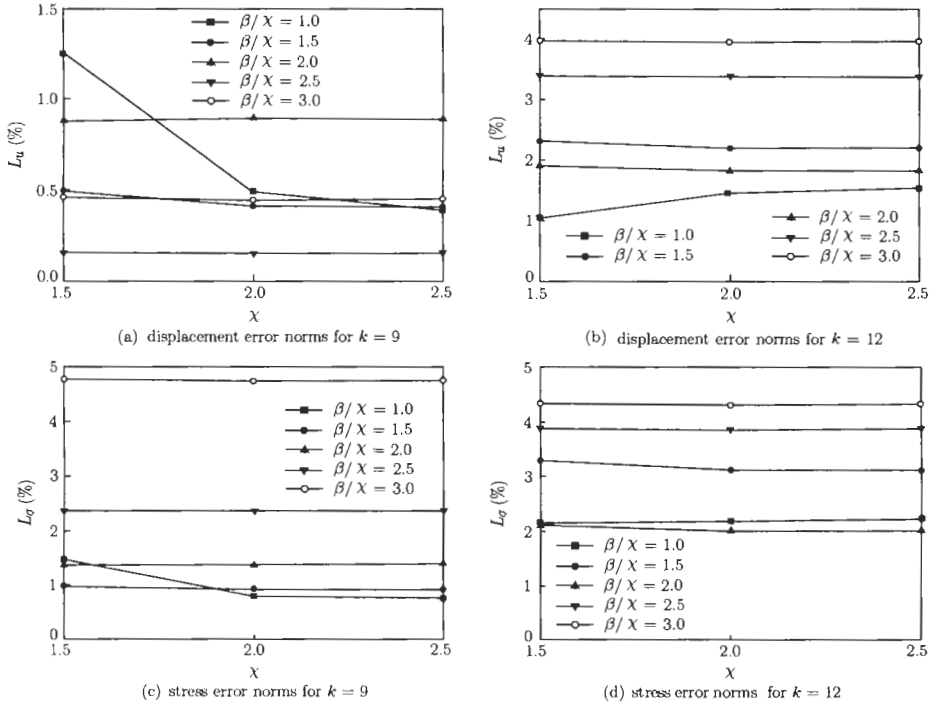

Fig. 2. Error norms obtained by using MWLS with weight function WF1.

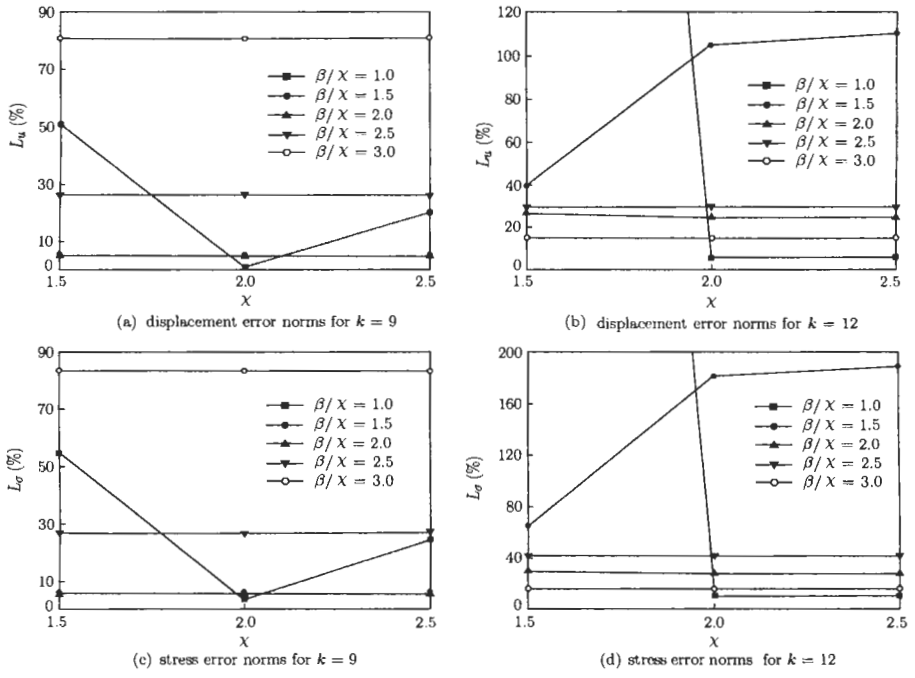

(a) displacement error norms for $k = 9$ (b) displacement error norms for $k = 12$

(c) stress error norms for $k = 9$ (d) stress error norms for $k = 12$

Fig. 3. Error norms obtained by using CBMM with weight function WF1.

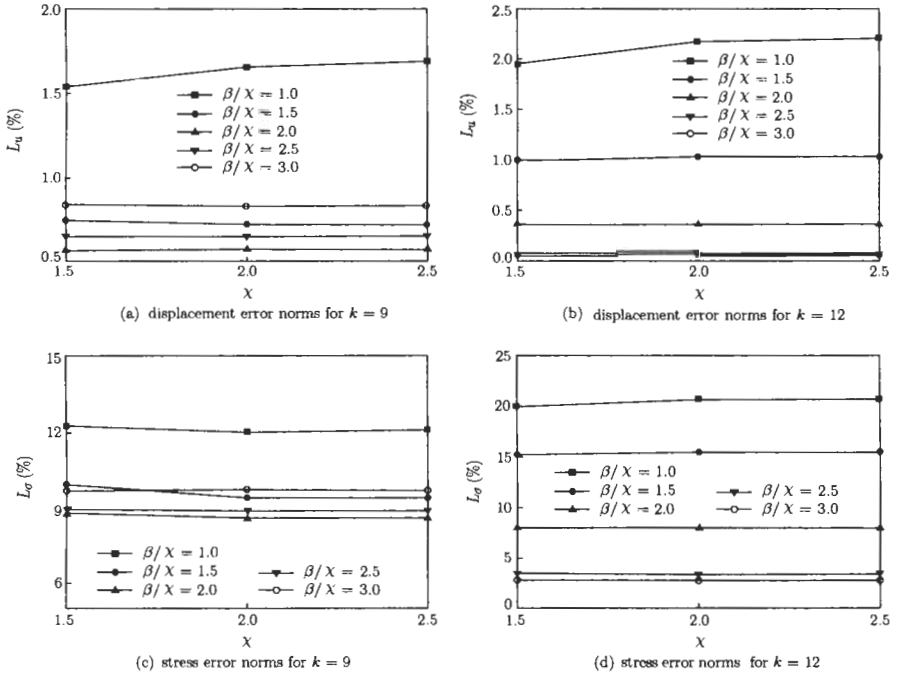

(a) displacement error norms for $k = 9$ (b) displacement error norms for $k = 12$

(c) stress error norms for $k = 9$ (d) stress error norms for $k = 12$

Fig. 4. Error norms obtained by using GBMM with weight function WF1.

This problem is analyzed with different parameters, such as k, χ, α and β, type of weight function and type of approximation. The exact analytical traction solution is prescribed on the right edge of the beam and the exact analytical displacement solution is imposed on the left edge. The upper and lower edges of the beam are traction-free.

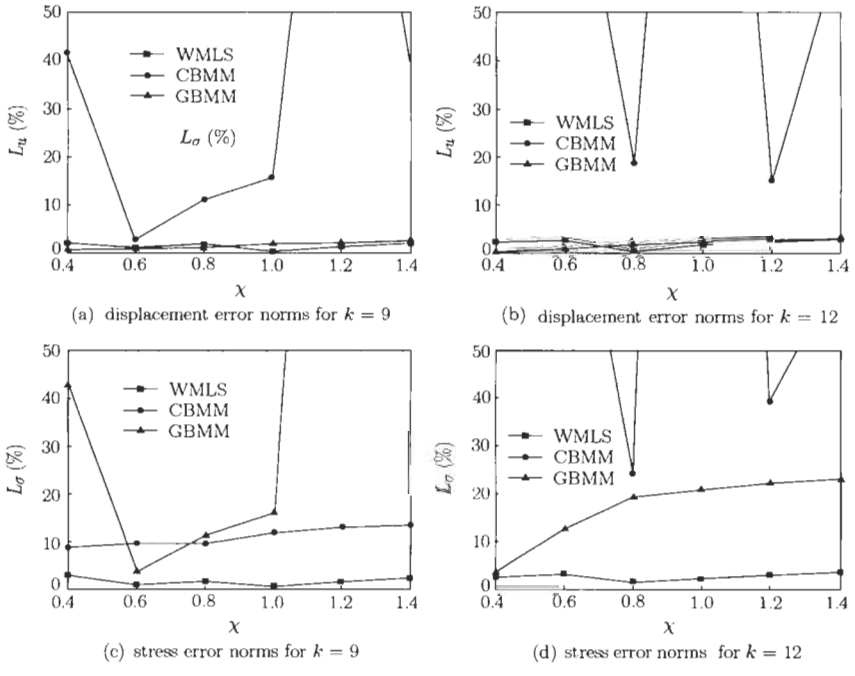

(a) displacement error norms for $k = 9$ (b) displacement error norms for $k = 12$

(c) stress error norms for $k = 9$ (d) stress error norms for $k = 12$

Fig. 5. Error norms obtained by using MWLS, CBMM and GBMM with weight function WF2.

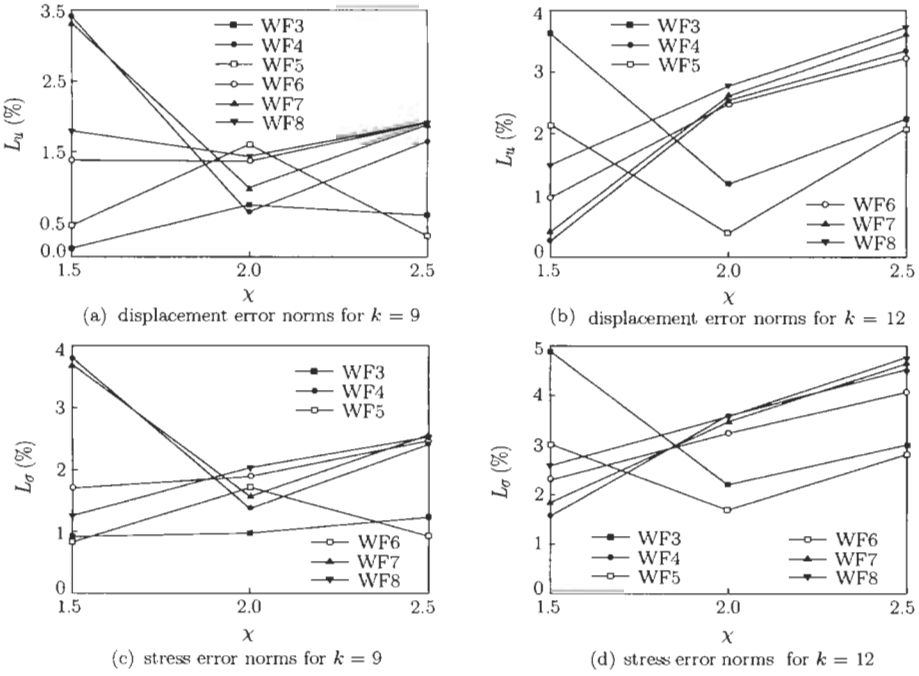

(a) displacement error norms for $k = 9$ (b) displacement error norms for $k = 12$

(c) stress error norms for $k = 9$ (d) stress error norms for $k = 12$

Fig. 6. Error norms obtained by using MWLS with weight function WF3-WF8.

Figures 2-8 compare the displacement and stress error norms obtained by using MWLS, CBMM and GBMM with different parameters. In all figures, (a) and (b) compare the error norms of displacement for $k = 9$ and $k = 12$, respectively, while (c) and (d) compare the error norms of stress for $k = 9$ and $k = 12$, respectively. In all GBMM computation, the 8×32 uniform background cell is used to integrate

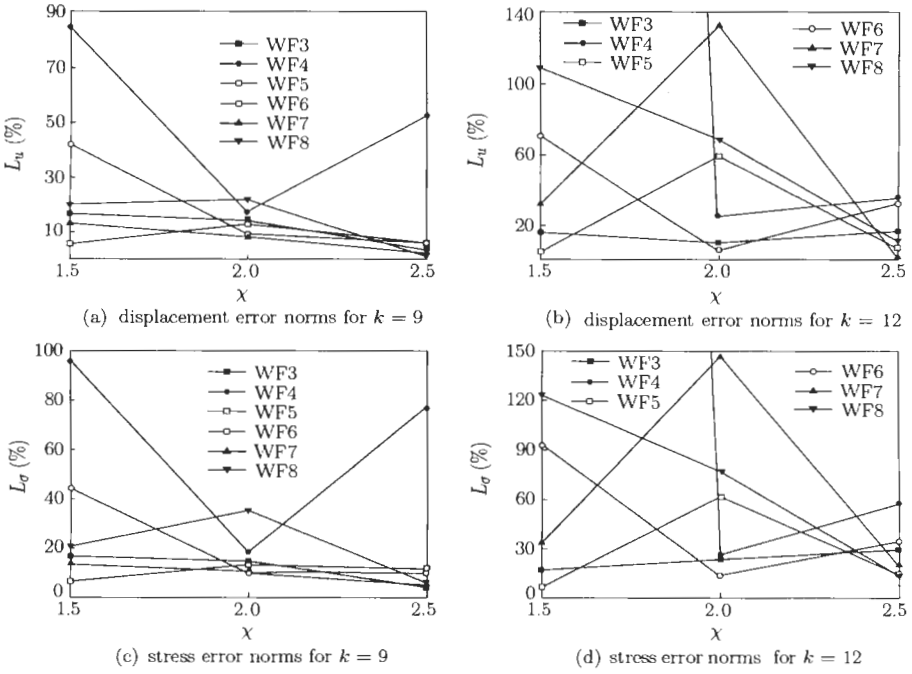

(a) displacement error norms for $k = 9$ (b) displacement error norms for $k = 12$

(c) stress error norms for $k = 9$ (d) stress error norms for $k = 12$

Fig. 7. Error norms obtained by using CBMM with weight function WF3-WF8.

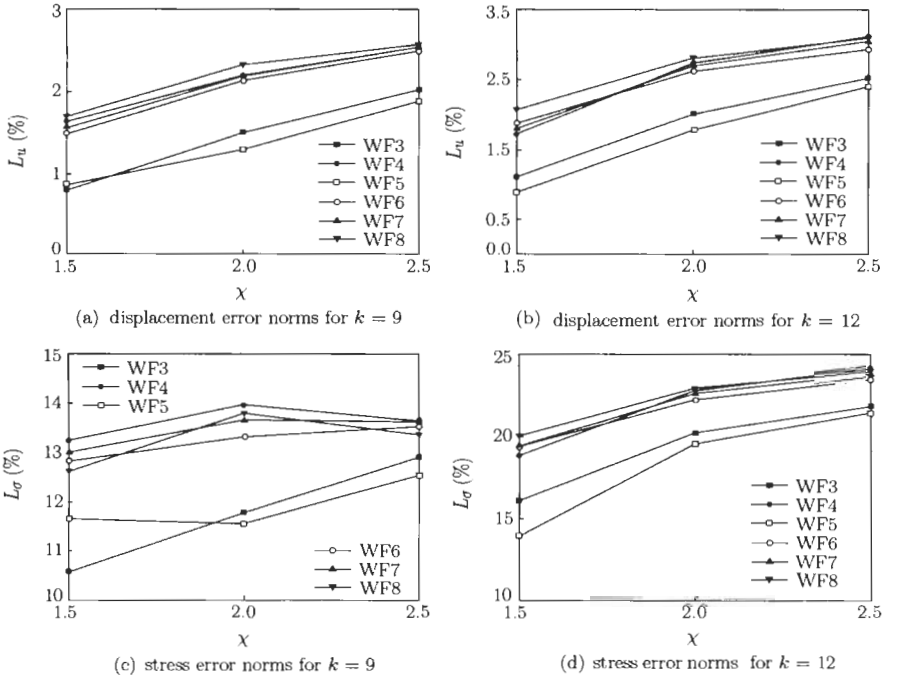

(a) displacement error norms for $k = 9$ (b) displacement error norms for $k = 12$

(c) stress error norms for $k = 9$ (d) stress error norms for $k = 12$

Fig. 8. Error norms obtained by using GBMM with weight function WF3-WF8.

the Galerkin weak form and the 3×3 Gauss quadrature is used in each cell. The essential boundary conditions are imposed by using the penalty method.

Figures 2-4 compare the error norms obtained by using MWLS, CBMM and GBMM with weight function WF1. It can be seen that the parameter β largely affects the results whereas χ has little effect

Table 1. **Error norms obtained by using LSQ for the cantilever beam**

	MWLS		CBMM		GBMM	
k	9	12	9	12	9	12
$L_u(\%)$	3.18	7.80	6.5	182	2.62	3.59
$L_\sigma(\%)$	3.77	12.06	7.08	294	12.8	25.6

on the results. It appears that different meshless methods have different optimum values of parameter β.

Figure 5 compares the error norms obtained by using MWLS, CBMM and GBMM with weight function WF2. It can be seen that the parameter α has significant effects on the results.

As is well known, CBMM is unstable and its results largely depend on the parameter β in WF1 and $\alpha \cdot \chi$ in WF2. For example, excellent displacements are obtained by using parameter $\alpha \cdot \chi = 0.6$, but very poor displacements are obtained with $\alpha \cdot \chi = 0.4$. In contrast, MWLS is stable.

Figures 6-8 compare the error norms obtained by using MWLS, CBMM and GBMM for weight functions WF3-WF8. They indicate that the type of weight functions has significant effect on the results of the meshless method. Consequently, the type of weight functions and parameters associated with them must be carefully chosen. Weight functions WF3 and WF5 lead to the best results for MWLS in this example. Parameter χ also has a significant effect on the weight functions WF3-WF8. $\chi = 2$ is recommended.

Table 1 compares the error norms obtained by using LSQ with different values of parameter k. Although LSQ approximation is less accurate than MLS approximation, it yields reasonable results. The accuracy of results obtained by using LSQ approximation can be improved by increasing the total number of nodes. In the analysis of impact and explosion, a large number of nodes are required to model the wave propagation properly. It is therefore sensible to use LSQ approximaiton to reduce the computational effort required.

In this numerical example, the displacement accuracy obtained by GBMM is slightly higher than that of MWLS, but the stress accuracy obtained by GBMM is lower than that of MWLS for $k = 9$ and

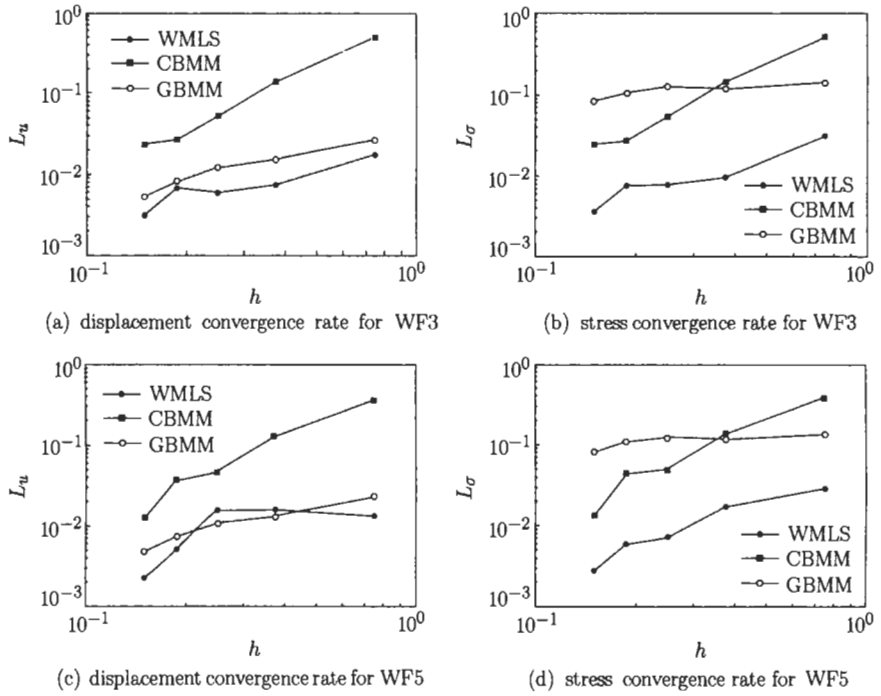

(a) displacement convergence rate for WF3 (b) stress convergence rate for WF3

(c) displacement convergence rate for WF5 (d) stress convergence rate for WF5

Fig. 9. Convergence rate for weight functions WF3 and WF5 with $k = 9$ and $\chi = 2.0$.

$k = 12$. As shown in Ref.[13], all nodes which cover the evaluation point $\boldsymbol{x}$ should be used to construct the MLS approximation to further improve the accuracy of stress in GBMM. However, the CPU time will be increased significantly owing to the significant increase of the number of neighbors of point $\boldsymbol{x}$.

Figure 9 compares the convergence rate of MWLS, CBMM and GBMM. (a) and (b) show the displacement and stress convergence rates for the weight function WF3, respectively, whereas (c) and (d) show the displacement and stress convergence rate for the weight function WF5, respectively. In this example, the displacement convergence rate of MWLS is comparable to that of GBMM. However, the stress convergence rate of MWLS is even higher than that of GBMM for $k = 9$.

In this numerical example, $k = 9$ leads to better results than $k = 12$ and, at the same time, reduces the computational effort significantly.

4.2. Infinite Plate with a Central Circular Hole

Consider the problem of an infinite plate with a central circular hole of radius a. The plate is subject to a uniform tension, σ_0, in the x direction at infinity. The exact solution of this problem is available[11]. Because of the symmetry, only the upper right quadrant of the plate is modelled and the overall dimension of the quadrant is $5a \times 5a$. A plane stress state is assumed with dimensionless elastic modulus $E = 1000$ and Poisson's ratio $\nu = 1/3$. In this analysis, σ_0 is taken to be 1. The exact analytical displacements solution is imposed on the left and bottom edges, whereas the exact analytical traction solution is imposed on the right and upper edges. The periphery of the circular hole is traction-free. The nodal arrangement is shown in Fig.10. Conclusions drawn from this numerical study are similar to those drawn from the previous example, so the numerical results of this example are not given in detail.

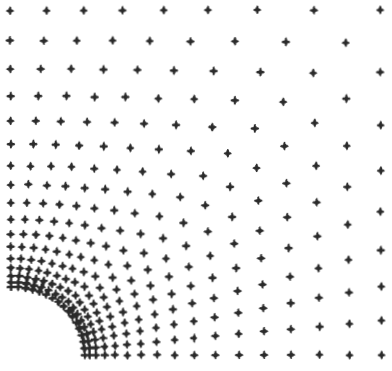

Fig. 10 Infinite plate discretized with 289 nodes.

V. CONCLUDING REMARKS

MWLS is critically examined with two numerical examples. With respect to the present numerical studies, the following conclusions can be drawn:

1. CBMM is not stable and its accuracy largely depends on the type of weight function, paramter k and χ. Unlike CBMM, MWLS appears to be stable. From the weighted residual method's point of view, the essential difference between CBMM and MWLS is how to handle the residuals of equilibrium equations at boundary nodes. The residuals of equilibrium equations at boundary nodes are simply ignored in CBMM, but are minimized in a weighted least square sense in MWLS. As revealed in this study, one of the possible reasons for the instability of CBMM is that the equilibrium conditions are not satisfied at the boundary nodes.
2. Weight functions have a significant effect on the results of meshless methods and, thus, have to be carefully chosen in an analysis. Although excellent results can be obtained by weight functions WF1 and WF2 with properly determined parameters α and β, it is difficult to determine the optimum value of parameters α and β. In the absence of undetermined parameters, weight functions WF3-WF8 are convenient to use in an analysis. Based on this study, weight functions WF3 and WF5 are recommended.
3. Parameter χ has a minor effect on the results of meshless methods for the weight functions WF1 and WF2, but has a significant effect for the weight functions WF3-WF8 in some cases. $\chi = 2$ is recommended.
4. Results with reasonable accuracy can be obtained by LSQ approximation which is much more efficient than MLS approximation. In the analysis of impact and explosion problems, a large number of nodes are required to model wave propagation properly. LSQ may be used to obtain satisfactory results at a much reduced computational effort.
5. Results obtained by using $k = 9$ are better than those by using $k = 12$ in most cases. Hence, $k = 9$ is recommended for MWLS.
6. In the cases of $k = 9$ and $k = 12$, the displacement accuracy and convergence rate obtained by MWLS is comparable to that obtained by GBMM. However, stress accuracy and convergence rate

obtained by MWLS are even higher than those obtained by GBMM. In GBMM, all nodes which cover the evaluation point $\boldsymbol{x}$ have to be used to construct the MLS approximation to improve the stress accuracy. The practice, however, increases the CPU time significantly.

7. Although MWLS yields more accurate results than GBMM, it appears that the results of MWLS are more sensitive than GBMM to the type of the weight function.
8. As mentioned by Jiang[12], Least-Square-based method has a unified formulation for the numerical solution of all types of partial differential equations. As long as the equations have a unique solution, the LS-based method always can determine a good approximate solution. LS-based method is able to simulate fluid dynamics problems in all flight regimes, from incompressible/subsonic through transonic, supersonic and hyper sonic.

References

[1] Belytschko,T., Krongauz,Y., Organ,D., Fleming,M. and Krysl,P., Meshless methods: an overview and recent developments, *Comput. Methods Appl. Mech. Engrg.*, Vol.139, 1996, 3-47.

[2] Duarte,C.A., A review of some meshless methods to solve partial differential equations, Technical Report 95-06, TICAM, The University of Texas at Austin, 1995.

[3] Chen,W. and Tanaka,M., New insights in boundary-only and domain-type RBF methods, *J. Nonlinear Sci. and Numer. Simulation*, Vol.1, No.3, 2000, 145-151.

[4] Johnson,G.R., Beissel,S.R. and Stryk,R.A.A., Generalized particle algorithm for hHigh velocity impact computations, *Comput. Mech.*, Vol.25, 2000, 245-256.

[5] Johnson,G.R., Stryk,R.A. and Beissel,S.R., SPH for high velocity impact computations, *Comput. Methods Appl. Mech. Engrg.*, Vol.139, 1996, 347-373.

[6] Belytschko,T. and Tabbara,M., Dynamic fracture using element-free Galerkin methods, *Int. J. Numer. Methods Engrg.*, Vol.39, 1996, 923-938.

[7] Chen,J.S. and Pan,C., A Lagrangian reproducing kernel particle method for metal forming analysis, *Comput. Mech.*, Vol.22, 1998, 289-307.

[8] Liu,W.K. and Hao,S., Multiple scale meshfree methods for damage fracture and localization, *comput. Mater. Sci.*, Vol.16, 1999, 197-205.

[9] Zhang,X., Lu,M.W. and Wegner,J.L, A 2-D meshless model for jointed rock structures, *Int. J. Numer. Methods Engrg.*, Vol.47, 2000, 1649-1661.

[10] Dolbow,J. and Belytschko,T., Numerical integration of the Galerkin weak form in meshfree methods, *Computational Mechanics*, Vol.23, 1999, 219-230.

[11] Zhang,X., Liu,X.H., Song,K.Z. and Lu,M.W., Least-square collocation meshless method, *Int. J. Numer. Methods Engrg*, Vol.51, 2001, 1089-1100.

[12] Jiang,B.N., The Least-Squares Finite Element Method-Theory and Applications in Computational Fluid Dynamics and Electromagnetics, Berlin: Springer, 1998.

[13] Zhang,X., Pan,X.F., Hu,W. and Lu,B.N., Meshless weighted least-squares method, In: Eberhardsteiner,J. and Mang,H.A. ed., Fifth World Congress on Computational Mechanics, Vienna, Austria, July, 2002.

[14] Onate,E., Idelsohn,S. and Zienkiewicz,O.C., A finite point method in computational mechanics: applications to convective transport and fluid flow, *Int. J. Numer. Methods Engr.*, Vol.39, 1996, 3839-3866.

[15] Zienkiewicz,O.C. and Taylor,R.L., The Finite Element Method (5th Edition), Butterworth-Heinemann, 2000.

[16] Timoshenko,S.P. and Goodier,J.N., Theory of Elasticity (3rd Edition), New York: McGraw-Hill, 1987.